IEEE Access
Multidisciplinary | Rapid Review | Open Access Journal

Received 21 June 2022, accepted 2 July 2022, date of publication 6 July 2022, date of current version 18 July 2022.

Digital Object Identifier 10.1109/ACCESS.2022.3188774

RESEARCH ARTICLE

MCPA: A Fast Single Image Haze Removal Method Based on the Minimum Channel and Patchless Approach

CHIOU-SHANN FUH, (Member, IEEE), AND TZU-CHIA TUNG

Department of Computer Science and Information Engineering, Graduate Institute of Networking and Multimedia, National Taiwan University, Taipei 10617, Taiwan

Corresponding author: Tzu-Chia Tung (d04944016@ntu.edu.tw)

This work was supported by the Ministry of Science and Technology of Taiwan, R.O.C., under Grant MOST109-2221-E-002-158-MY2 and Grant MOST108-2221-E-002-140; in part by the Test Research, Jorgin Technologies, III; in part by Chernger; in part by Otus Imaging; in part by Jeilin Technology; in part by D8AI; in part by PSL; and in part by LVI.

ABSTRACT The image haze removal algorithm is challenging regarding computational processing speed and the hazy removal effect. Instead of using the local patch approach, which assumes the scene transmission to be locally constant and uses various filters to smooth the transmission map, this paper proposes a fast single image haze removal method based on a minimum channel and patchless approach. A new simple approach to estimate the atmospheric light and the scene transmission is proposed based on the minimum channel of images. The histogram of the minimum channel of the image is used to extract the atmospheric light pixels and exclude the non-hazy bright pixels in the image. The histogram equalization and image multiplication are applied to achieve better visual quality. In order to verify the performance of the proposed method, 100 images are collected from datasets I-HAZE, O-HAZE, and websites. Experimental results show that our proposed method outperforms up-to-date state-of-the-art haze removal algorithms using quantitative evaluations. From subjective comparisons, the proposed method outperforms most current haze removal algorithms in color restoration. Also, time assessment results show that our proposed method is the fastest among the up-to-date state-of-the-art haze removal methods and is about 15 times faster than the second-fastest method. The main contribution of the proposed method is significantly reducing computation time because it uses a patchless approach that does not need any filter and complicated algorithms. In addition to significantly reducing the computational processing speed, our proposed method can achieve better visual quality.

INDEX TERMS Atmospheric light, haze removal, patchless, scene transmission, single image.

I. INTRODUCTION

Poor quality images are often produced when capturing images in bad weather conditions, such as smoke, haze, rain, snow, and so on. Since the density of haze varies depending on the location, fog is difficult to detect in image processing. Therefore, the image haze removal algorithm is challenging and has attracted much attention in recent years. In order to solve the effect of fog on the image, many researchers have proposed haze removal algorithms to restore it as similar as possible to the original image taken under clear weather conditions.

Researchers classify image haze removal techniques into traditional non-learning-based and learning-based methods. In the early days, traditional non-learning methods were based on histogram techniques to remove haze from a single image [1]–[3]. However, a hazy single image cannot provide more information, resulting in a limited haze removal effect. Tan *et al*. [4] proposed a dehazing method based on a Markov random field that maximizes local contrast while assuming a

The associate editor coordinating the review of this manuscript and approving it for publication was Felix Albu.

layer of smooth airlight. This method produces compelling results with enhanced scene contrast. However, some halos at depth discontinuities are produced, which tend to be oversaturated. The method proposed by Fattal *et al*. [5] assumes that the albedo and medium transmittance of the scene is estimated under the condition that the transmittance and surface shading in the image are uncorrelated. However, it only effectively restores the image when the amount of haze is small enough, but it produces distortion in the severely blurred image caused by the hazy environment. In recent years, Dark Channel Prior (DCP) [6]–[8] is often used to dehaze the image. DCP makes the assumption that the intensity of the dark channel is higher in the hazy region. On the other hand, the intensity value of the dark channel in the haze-free region is very low, even close to zero. However, the fact is that the dark channel values for the sky areas without haze are much greater than zero. Thus, the recovered sky area is usually distorted, causing DCP not to recover the sky area in the image very well. Many algorithms have been developed to solve the shortcomings of DCP [9], [10], overcoming its slow processing speed and unpredictable performance in sky areas.

Yu *et al*. [11] proposed a dehazing method for a single scene image based on a fast bilateral filter method. Meng *et al*. [12] modeled the inherent boundary constraint on the transmission function and a weighted L1-norm into an optimization problem to estimate the unknown transmission. An efficient variable splitting algorithm was also proposed to solve the optimization problem. Sulami *et al*. [13] proposed an automatic method for recovering the atmospheric light vector in a single hazy image. The atmospheric light vector's orientation was recovered by exploiting the abundance of small image patches. The max-brightness transmission invariance was introduced, and a simple procedure for estimating the magnitude of the atmospheric light using this image prior was proposed. Wang *et al*. [14] proposed a fast single image haze removal algorithm based on a linear relationship in the minimum channel between the hazy image and the haze-free image. The transmission map was estimated based on a linear mode without exponential operations or sample training. Therefore, it can be easy to realize and has less computational complexity. The experimental results showed that the phenomena of over-saturation and halo effects could be avoided. Zhang *et al*. [15] proposed a dehazing algorithm that preserves naturalness using hue, saturation, and value color space. Khmag *et al*. [16] used the mean vector L2-norm to estimate the transmission map. A second-generation wavelet transform filter enhanced the estimated transmission map and filtered those outliers and unwanted artifacts. Shin *et al*. [17] proposed a dehazing algorithm that combines an image's radiance and reflectance components. Hu *et al*. [18] proposed a method based on the observation of uneven illumination, which replaces the global atmospheric light in the atmospheric scattering model with the local illumination estimation method of the blurred image. Zheng *et al*. [19] proposed an image dehazing scheme to eliminate haze's visual degradation effectively. A multi-exposure image fusion scheme based on adaptive structure decomposition to each image patch was applied to fuse different exposure-level images into a haze-free image. Zhu *et al*. [20] proposed an image fusion algorithm to enhance the performance of image dehazing. Pixelwise weight maps were established using global and local exposures to guide the fusion process based on gamma-corrected underexposed images. Li *et al*. [21] proposed globally guided image filtering to preserve the fine structure of the dehazed image. Experimental results showed that the proposed haze removal method can improve visual quality. Zhao *et al*. [22] proposed a single image dehazing method by analyzing the prior information of local dehazed patches. A transmission was estimated accurately based on the local patch. Weighted interpolation and guided filtering were applied to refine the edges and details of the transmission map.

Recently, there have been an increasing number of learning-based methods that can achieve accurate and fast haze removal, such as employing random forests [23], color attenuation [24], [25], and deep learning [26]–[38]. DehazeNet [39] developed a convolutional neural network to estimate the transmission map of hazy images and then restore haze-free images by estimating atmospheric light. Ren *et al*. [40] designed a multiscale convolutional neural network to improve the haze removal performance for a single image by learning more features. In deep learning-based methods, large-scale haze image pairs and corresponding haze-free images must be prepared, and their relations must be trained to make the model aware of the haze-free images. However, learning-based methods achieve good results for images with uniform haze distribution. The desired effect cannot be achieved for those images whose haze distribution is disproportionate. Moreover, the dehazing accuracy of deep learning-based methods depends on the amount of data. In reality, it is difficult to capture both foggy and fog-free images in the same frame. Therefore, these learning-based methods' contrast enhancement of images is insufficient. Due to the limitation of the training dataset, it might not effectively adapt to various real-world environments.

In the DCP-based haze removal algorithm, the dehazing performance depends on the local patch size that needs to be tuned [41]. Also, the transmission map can cause problems such as false textures and blocking artifacts and decrease the dark channel's apparent resolution due to the local patch [24]. Therefore the transmission map needs refining subsequently by using a filter such as Gaussian filter [42]–[44], bilateral filter [11], [45], soft matting [6], cross-bilateral filter [46], [47], adaptive filter [48], second-generation wavelet filter [16], or guided filter [43], [49]–[51]. However, it increases computational complexity and suffers from other artifacts [9].

In order to solve the problems that the state-of-art haze removal patch-based methods will increase computational complexity and suffer from artifacts, a new patchless atmospheric light estimation approach and a new simple patchless transmission estimation approach are proposed in this paper.

The main contribution of the proposed method is significantly reducing the computational processing speed and achieving a significant dehazing effect, including color restoration.

The remainder of this paper is organized as follows. Section II introduces related works to understand our proposed method. In Section III, the details of the proposed dehazing method (MCPA) are illustrated. Section IV presents and analyzes the experimental results. Finally, the results are summarized in Section V.

II. RELATED WORKS

A hazy image can be mathematically expressed as an atmospheric scattering modeled as follows [52]:

$$I(x) = J(x)e^{-\beta d(x)} + A\left(1 - e^{-\beta d(x)}\right), \tag{1}$$

where x is the pixel coordinates; I denotes the hazy image; J represents the haze-free image; A denotes the global atmospheric light; β is the scattering coefficient of the atmosphere; and d is the depth of scene. The scene transmission is expressed as

$$t\,(x) = e^{-\beta d(x)}. \tag{2}$$

In the DCP-based haze removal algorithm [6], the dark channel is defined as

$$I^{dark}(x) = \min_{y\in\Omega(x)}\left(\min_{c\in\{r,g,b\}} I^c(y)\right), \tag{3}$$

where I^c is an intensity of a color channel $\{r, g, b\}$ of the image, and $\Omega(x)$ represents a local patch centered at pixel x.

The dark channel of a hazy image is expressed as

$$\min_{y\in\Omega(x)}\left(\min_{c}\frac{I^c(y)}{A^c}\right) = \tilde{t}(x)\min_{y\in\Omega(x)}\left(\min_{c}\frac{J^c(y)}{A^c}\right) + (1-\tilde{t}(x)). \tag{4}$$

The atmospheric light can be estimated from the dark channel Eq. (4) as

$$\min_{y\in\Omega(x)}\left(\min_{c}\frac{I^c(y)}{A^c}\right) \approx 1 \text{ and } \tilde{t}(x) \approx 0. \tag{5}$$

After estimating the atmospheric light, the transmission map can be obtained from the dark channel Eq. (4) as

$$\tilde{t}(x) = 1 - \min_{y\in\Omega(x)}\left(\min_{c}\frac{I^c(y)}{A^c}\right) \text{ for } \min_{y\in\Omega(x)}\left(\min_{c}\frac{J^c(y)}{A^c}\right) \approx 0. \tag{6}$$

The transmission map needs further refinement by using a filter due to the local patch approach, and the haze-free image is finally recovered as

$$J(x) = \frac{I(x) - A}{max(\tilde{t}(x), t_0)} + A. \tag{7}$$

The DCP approach cannot well handle sky images and has high computational processing speed. Since the DCP has block artifacts due to the local patch approach, the transmission map needs to be refined by Laplacian-based soft matting [53]. Due to high computational processing speed and time consumption, many researchers have developed faster image filtering to replace Laplacian-based soft matting, including median filtering [54], constant time bilateral filtering [55], and gain intervention refinement filtering [56].

Many researchers [9], [24] estimated the haze density of hazy images to obtain the scene transmission. Peng *et al.* [9] estimated haze density d based on the fact that haze density is correlated with its minimum/maximum channel and their difference as

$$d \propto I_{min} \propto (I_{max} - I_{min}), \tag{8}$$

$$I_{max} = \max_{c\in\{r,g,b\}} I^c(x), \tag{9}$$

$$I_{min}(x) = \min_{c\in\{r,g,b\}} I^c(x). \tag{10}$$

Haze density d can be estimated as

$$d(x) = I_{min}(x)\left(1 - \frac{I_{max}(x) - I_{min}(x)}{max(1, I_{max}(x))}\right). \tag{11}$$

The scene transmission t is assumed to be uniform in a small local patch $\Omega(x)$ and can be estimated as

$$t(x) = 1 - \omega F_{gif}\left(\min_{y\in\Omega(x)} d(y)\right), \tag{12}$$

where F_{gif} is the guided image filtering [57], and ω is a parameter whose range is usually set to be 0.95 to 1.

Zhu *et al.* [24] developed a linear model to estimate the depth of the scene and constructed a depth map as follows:

$$d(x) = \theta_0 + \theta_1 v\,(x) + \theta_2 s\,(x) + \varepsilon(x), \tag{13}$$

where x is the pixel coordinate of the image; d denotes the scene depth; v represents the brightness component of the hazy image; s denotes the saturation component; θ_0, θ_1, θ_2 are the linear coefficients which can be estimated by using the gradient descent algorithm; $\varepsilon(x)$ denotes the random error of the model; and ε denotes a random image.

It can be seen that the algorithms of the above two scene transmission estimation methods are too complicated, and both are based on the local patch approach and require the use of filters, which results in excessive computation and causes artifacts. Motivated by the related works, this paper develops a simple algorithm based on the minimum channel without using the local patch to estimate the scene transmission.

In order to solve the problem that the white object in the mage will result in an inaccurate estimation of the atmospheric light, Peng *et al.* [9] used local minimum filtering to remove isolated peaks in the Probability Mass Function (PMF) calculated from the image histogram based on the fact that non-hazy bright pixels are usually brighter than airlight pixels and the number of airlight pixels is much more than that of non-hazy bright pixels.

The local minimum filtering of a 1-D minimum operation P_m was developed to the PMF of the minimum channel and is expressed as

$$P_m(l) = \min_{-r\le s\le r}\left(P_V(l+s)\right), \tag{14}$$

where P_V denotes the PMF of the minimum channel, l is a value from 0 to 255, and r setting to 5 represents the radius for the operation.

Since non-hazy bright pixels in the PMF calculated from the image histogram for haze images may not be isolated, the local minimum filtering cannot remove non-hazy bright pixels. Motivated by this related work, this paper develops a simple algorithm based on the minimum channel of a histogram to remove non-hazy bright pixels for the atmospheric light estimation.

Histogram equalization [58] is one of the common algorithms for enhancing digital image contrast. Histogram equalization uses the probability and summation of the intensity level of the digital input image to perform intensity mapping to redistribute the histogram to make the digital image distribution uniform. The probability of occurrences of intensity level r_i can be expressed as

$$pr(r_i) = \frac{n_i}{n}, \quad i \in 0, \ldots, L-1, \tag{15}$$

where n_i represents the number of occurrences of pixels having intensity level r_i; n is the total number of pixels in the entire image; and L is the number of all the intensity levels in the image.

The histogram equalization transformation function for discrete mapping can be expressed as

$$T(r_k) = (L-1)\sum_{j=0}^{k}\frac{n_j}{n}. \tag{16}$$

The output of intensity level s for every pixel corresponding to the intensity level r of the input image can be expressed as

$$s_k = T(r_k). \tag{17}$$

This paper proposes to use simple histogram equalization to enhance image contrast to obtain better visual quality.

III. OUR PROPOSED METHOD (MCPA)

This section introduces the proposed method in detail. The flowchart of the proposed method is shown in Fig. 1. Two hazy images are given as examples to illustrate the proposed algorithm as follows. First, the minimum channel values are calculated from RGB channels of the input image. The atmospheric light and the scene transmission can be estimated from the minimum channel. The histogram of the minimum channel is used to determine whether there exist non-hazy pixels or not and extract pixels corresponding to the atmospheric light in the histogram. Two cases are given to illustrate how to extract pixels corresponding to atmospheric light. One case is for the existence of non-hazy pixels, and the other is not. The red vertical line in the histogram shows the position corresponding to the atmospheric light. The red dots in the red boxes and the zoom-in figures on the right side of the histograms show the extracted atmospheric light pixels in the original images. After estimating the atmospheric light and the transmission, the scene radiance can be recovered. Histogram equalization is applied to enhance the contrast of the dehazed image. Finally, to solve over-enhanced image problem, each pixel of the enhanced RGB image is multiplied by the correspondent pixel of the original image to obtain the final dehazed result.

A. ESTIMATION OF THE ATMOSPHERIC LIGHT A

DCP [6] used the dark channel to find the most haze-opaque region. The top 0.1 percent brightest pixels in the dark channel were first picked. These pixels with the highest intensity in the input image I are picked as the atmospheric light. However, accurate atmospheric light may not be found when there exist non-hazy bright pixels such as larger white objects, LED (Light Emitting Diode), billboard or headlight. Although a larger patch size may be used to calculate the DCP to get less problematic for estimating atmospheric light, the apparent resolution of the dark channel is inevitably decreased as the size of the patch increases [41]. Also, automatically finding an appropriate patch size to calculate the DCP for estimating atmospheric light is difficult [9].

Zhu *et al.* [24] used a depth map to estimate atmospheric light. In order to solve the problem that the white object in the mage will result in an inaccurate estimation of the depth, the scene depth needs to be locally constant, and the raw depth map is expressed as

$$d_r(x) = \min_{y\in\Omega(x)} d(y), \tag{18}$$

where $r(x)$ is an $r \times r$ neighborhood centered at x, and d_r is the depth map with scale r.

The top 0.1 percent brightest pixels in the depth map were picked, and the pixels with the highest intensity among these brightest pixels in the corresponding hazy image I were selected as the atmospheric light A.

Since the estimation of the atmospheric light based on the local patch will result in the artifacts in the image, guided image filtering is used to smooth the image [24]. It is noted that using the guided image filter will significantly increase the computational processing speed. In order to overcome the above-mentioned problems, a new atmospheric light estimation approach is proposed without using local patches. The estimation of the atmospheric light is illustrated as follows.

The minimum channel of $J^c(x)$ can be expressed as

$$\min(I(x)) = I_{min}(x) = \min_{c\in\{r,g,b\}}\left(J^c(x)t(x) + A^c(1-t(x))\right). \tag{19}$$

The maximum intensity of the minimum channel of $J^c(x)$ can be expressed as

$$\max_{y\in I(x)}\left(I_{min}(y)\right) = \max_{y\in I(x)}\left(\min_{c\in\{r,g,b\}} J^c(y)t(x) + A(1+t(x))\right). \tag{20}$$

The atmospheric light A can be estimated from the pixel with the highest minimum channel value as follows:

$$A = I\left(argmax_{y\in I(x)}\left(I_{min}(y)\right)\right). \tag{21}$$

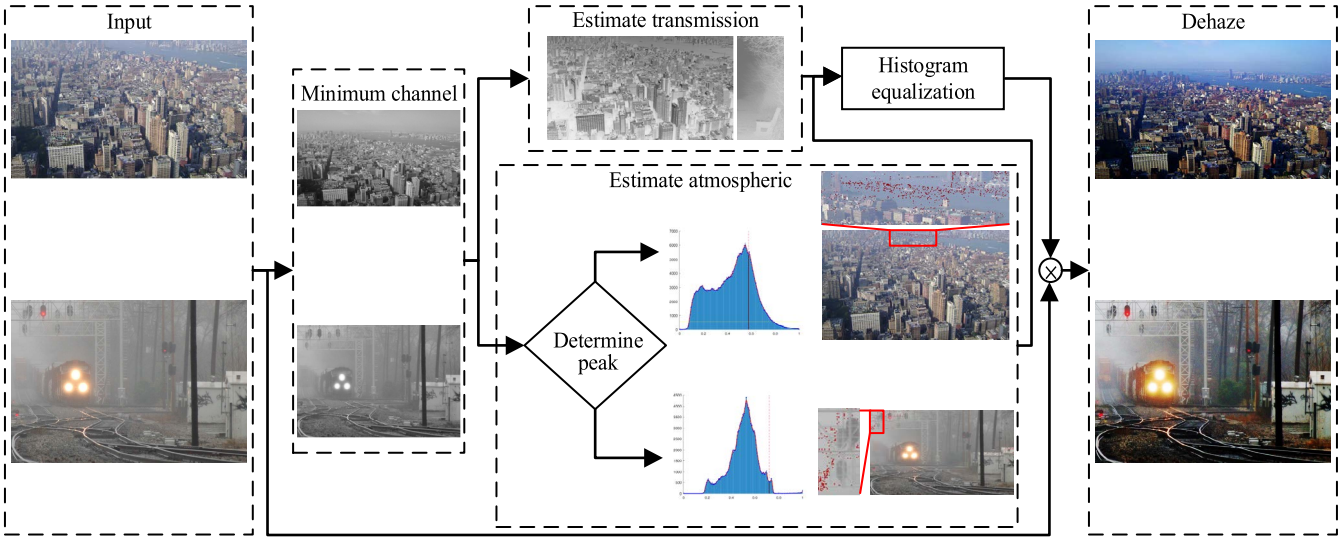

FIGURE 1. Flow chart of our proposed method.

Since $\max_{y \in I(x)} (I_{min}(y))$ and the related top 0.1% brightest pixels represent the pixels corresponding to the atmospheric light pixels or the non-hazy bright pixels in the image; only the atmospheric light pixels need to be extracted.

Instead of using probability, let $p(r_k)$ be the number of occurrences of pixels having intensity level r_i in the histogram of the minimum channel of $J^c(x)$ of the image.

$$p(r_k) = n_k \text{ for } k = 0, 1, 2, \ldots, 255, \tag{22}$$

where r_k denotes the k_{th} intensity level, and n_k is the number of pixels in the image with intensity level r_k.

Usually, the image histogram has discrete values and is zigzag. A smoothing spline is used to fit the histogram to obtain a smoothed curve, as shown in Fig. 2(b). After curve fitting the peak values of the image histogram, a Matlab function is applied to the histogram curve to find two local maximums and one local minimum, which is located between the two local maximums corresponding to the three largest intensity values in the histogram. The number of non-hazy bright pixels is much less than that of the atmospheric light pixels. The intensity levels of non-hazy bright pixels are higher than that of the atmospheric light pixels. Thus, the atmospheric light can be automatically determined by averaging RGB pixel values corresponding to the local minimum for the case that the last local maximum value is much less than the second last local maximum value. Otherwise, the atmospheric light is estimated by averaging the RGB pixel values corresponding to the top 0.1 percent brightest pixels in the histogram.

Fig. 2(a) shows a haze image with three headlights. Fig. 2(b) shows the curve fitted histogram $p(r_k)$ of the minimum channel of $J^c(x)$ of the image shown in Fig. 2(a). Two local maximums and one local minimum, which is located between the two local maximums, corresponding to the three largest intensity values, are found in the histogram. The last local maximum value is much less than the other local maximum value. The atmospheric light can be automatically determined by averaging the RGB pixel values corresponding to the local minimum (red dot line), as shown in Fig. 2(b). Figs. 2(c)-(e) show the comparison of three different estimation methods of atmospheric light. Figs. 2(c) and 2(d) show the region in red color from which the DCP method and CAP method obtain the atmospheric light, respectively. It can be seen that both dark channel and depth map methods select the headlights to estimate atmospheric light.

Fig. 2(e) shows the region in dotted red color from which our method estimates the atmospheric light. Obviously, our method can accurately estimate atmospheric light compared with the other two methods.

Fig. 3(a) shows a haze image without LED light or white objects. Fig. 3(b) shows the curve-fitted histogram $p(r_k)$ of the minimum channel of $J^c(x)$ of the image shown in Fig. 3(a). It can be seen that two local maximums and one local minimum between the two local maximums are found in the histogram. However, the last local maximum value is not much less than the other local maximum value. In this case, the atmospheric light is estimated by averaging the RGB pixel values corresponding to the top 0.1 percent brightest pixels in the histogram.

Figs. 3(c) and 3(d) compare three different methods of estimation of atmospheric light. Figs. 3(c) and 3(d) show the region in red color from which the DCP method and CAP method obtain the atmospheric light, respectively. Fig. 3(d) shows the region in dotted red color from which our method estimates the atmospheric light. It can be seen that all three methods can accurately estimate atmospheric light. However, our proposed method (MCPA) is efficient and straightforward without using the local patch and thus does not need to use any

FIGURE 2. An example of applying histogram to the image with three headlights to estimate the atmospheric light and the comparison results (a) Original image, (b) Histogram. Atmospheric light estimation results using (c) DCP, (d) CAP (Color Attenuation Prior), and (e) our proposed method (MCPA).

FIGURE 3. An example of applying histogram to the image to estimate the atmospheric light and the comparison results (a) Original image (b) Histogram. Atmospheric light estimation results using (c) DCP, (d) CAP, and (e) our proposed method (MCPA).

filter subsequently in comparison with the other two methods or state-of-art methods.

B. ESTIMATION OF THE TRANSMISSION

Based on the assumption that the haze density of a hazy image correlates with its minimum channel, the proposed haze density d can be estimated as [9]

$$d\,(x) = \omega I_{min}\,(x)\,, \tag{23}$$

where $I_{min}\,(x)$ is obtained from Eq. (14).

The proposed scene transmission t can be estimated as

$$t(x) = 1 - (\omega I_{min}(x))\,. \tag{24}$$

Lee *et al*. [41] reported that using ω around 0.9, the under-estimation of the transmission map is considerably decreased. Compared with Eq. (6), it can be seen that the proposed simplified scene transmission t needs to decrease the value of ω to compensate for the under-estimation of scene transmission. Through experimental study, it is found that letting the value of ω be 0.85 can achieve better visual quality. The proposed estimate transmission can be expressed as

$$t(x) = 1 - (0.85 \times I_{min}(x))\,. \tag{25}$$

Compared with the state-of-art transmission estimation methods for hazy images, our proposed method (MCPA) is significantly efficient due to only using the minimum channel.

C. RECOVERING THE SCENE RADIANCE

After estimating the atmospheric light and the transmission, the scene radiance can be recovered as

$$J\,(x) = \frac{I\,(x) - A}{\max\,(t(x), 0.01)} + A, \tag{26}$$

where $t(x)$ is obtained from Eq. (16). It is noted the recovery equation will decrease the intensity level for the pixels if its value is less than the atmospheric light. Otherwise, the intensity level for the pixels will be increased if its value is larger than the atmospheric light. Thus, the recovery equation usually makes the image darker or brighter. To solve the problem, this paper proposes to use a simple histogram equalization as shown in Eq. (9) to enhance image contrast.

Finally, to solve the over-enhanced image problem, each pixel of the enhanced RGB image is multiplied by the correspondent pixel of the original image to obtain the final dehazed result. The multiplication of the two RGB images is a pointwise operation and can be expressed as

$$I_{out}\,(i,j) = I_{org}\,(i,j) \times I_{enh}\,(i,j)\,, \tag{27}$$

where I_{out}, I_{org}, and I_{enh} denote the output image, the original image, and the enhanced image, respectively.

IV. EXPERIMENTAL RESULTS

In this section, Figs. 4-10 represent the performance comparison of our proposed dehazing method (MCPA) with some up-to-date state-of-the-art methods, including FVR [59], DCP [6], BCCR [12], ATM [13], CAP [24], DehazeNet [39], PAD-MEF [19], Zhu *et al*. [20], Zhao *et al*. [22], and Li *et al*. [21]. In order to verify the performance of the proposed method, 100 images are collected from I-HAZE [60], O-HAZE [61], and websites that had more white or gray areas in the real world and clearly had haze. The dataset I-HAZE and O-HAZE comprise 75 hazy images. Twenty-five hazy images are collected from websites. The sizes of the images are from 600 × 450 pixels to 2,833 × 4,657 pixels. The two images on the left and right below each image are the enlarged images corresponding to the regions of the red box and the blue box in the image, respectively. For a fair comparison, the advanced state-of-the-art dehazing methods are implemented

FIGURE 4. Subjective comparisons of different methods on images: (a) Input hazy image, (b) FVR, (c) DCP, (d) BCCR, (e) ATM, (f) CAP, (g) DehazeNet, (h) PADMEF, (i) Zhu *et al.*, (j) Zhao *et al.*, (k) Li *et al.*, and (l) Our MCPA.

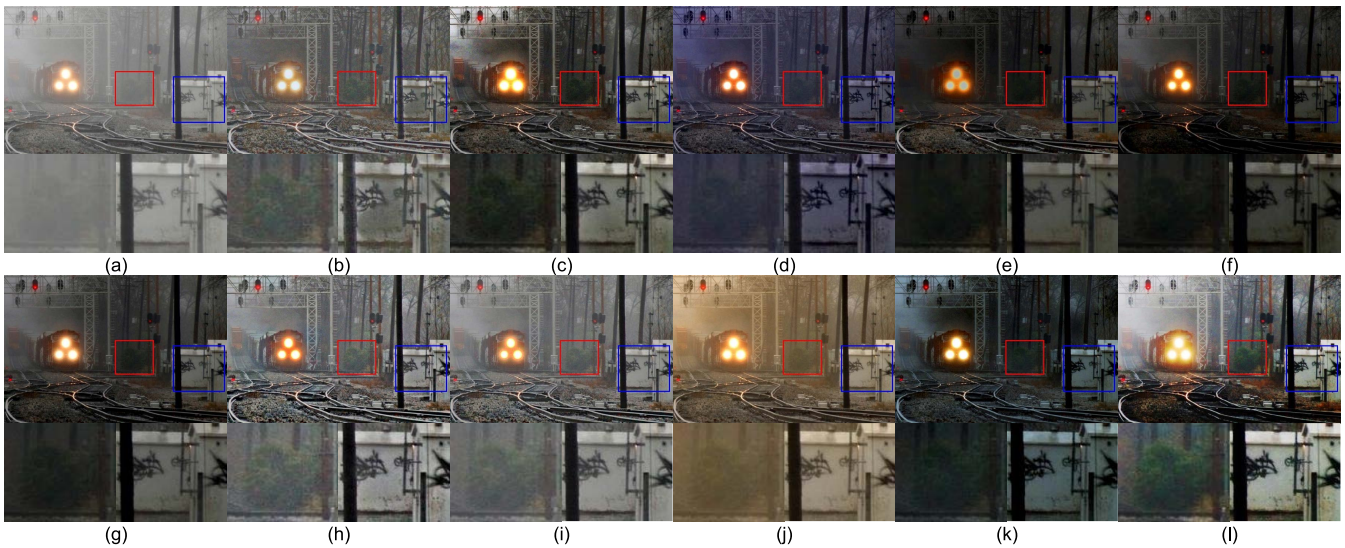

FIGURE 5. Subjective comparisons of different methods on images: (a) Input hazy image, (b) FVR, (c) DCP, (d) BCCR, (e) ATM, (f) CAP, (g) DehazeNet, (h) PADMEF, (i) Zhu *et al.*, (j) Zhao *et al.*, (k) Li *et al.*, and (l) Our MCPA.

using the public code provided by the authors, and the parameters are set as default. The software environment used for the experiment is Matlab 2020a version. The computer specification used in this experiment is an Intel Core i9-9900X CPU of 3.60GHz and a memory of 64GB. Next, our experiments are divided into subjective comparisons, objective quality assessments, and running time assessments. Experimental details are described in detail in the following subsections.

A. SUBJECTIVE COMPARISONS

In subjective comparisons, our method (MCPA) is compared with up-to-date state-of-the-art dehazing algorithms. Fig. 4(a) illustrates one of the images where the haze distribution occupies almost the entire image, and the colors look dull. Therefore, many state-of-the-art dehazing algorithms cause the color of the girl's hair and face to be distorted because the original image's color cannot be accurately restored. For example, the images restored in Figs. 4(b)-4(d), and 4(k) are over-enhanced, such as girl's face turning brown. Fig. 4(e) shows that color distortion appears in the restored image. Figs. 4(f)-4(i) successfully remove fog. The defogging effect of Fig. 4(j) is not ideal, where the background and the girl's face and hair details are not obvious. Fig. 4(l) shows the results of our proposed method (MCPA). The enlarged image shows that the background details are successfully displayed,

FIGURE 6. Subjective comparisons of different methods on images: (a) Input hazy image, (b) FVR, (c) DCP, (d) BCCR, (e) ATM, (f) CAP, (g) DehazeNet, (h) PADMEF, (i) Zhu *et al.*, (j) Zhao *et al.*, (k) Li *et al.*, and (l) Our MCPA.

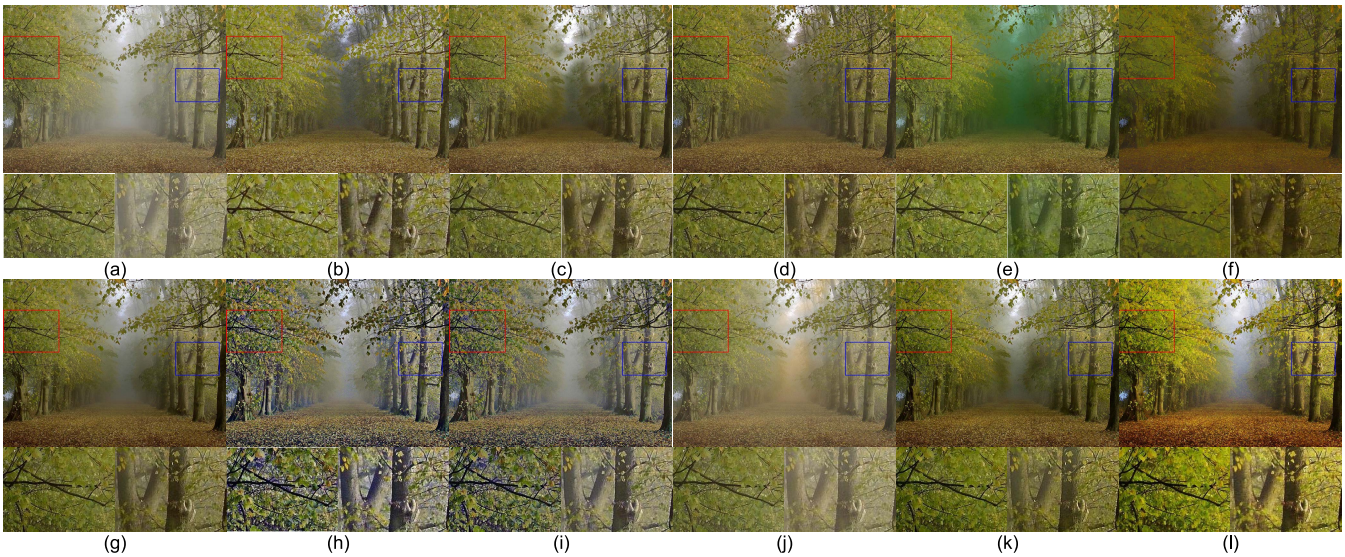

FIGURE 7. Subjective comparisons of different methods on images: (a) Input hazy image, (b) FVR, (c) DCP, (d) BCCR, (e) ATM, (f) CAP, (g) DehazeNet, (h) PADMEF, (i) Zhu *et al.*, (j) Zhao *et al.*, (k) Li *et al.*, and (l) Our MCPA.

and the girl's face is obviously more natural than other advanced state-of-the-art haze removal methods.

Fig. 5(a) shows the image with highly cluttered objects and excessive fog with three headlights. Although the method in Fig. 5(b) successfully removes the haze and objects hidden by the fog are revealed. Figs. 5(d) and 5(j) produce unrealistic tones, such as too much blue and yellow in the overall scene. The methods of Figs. 5(c), 5(e)-5(g), and 5(k) result

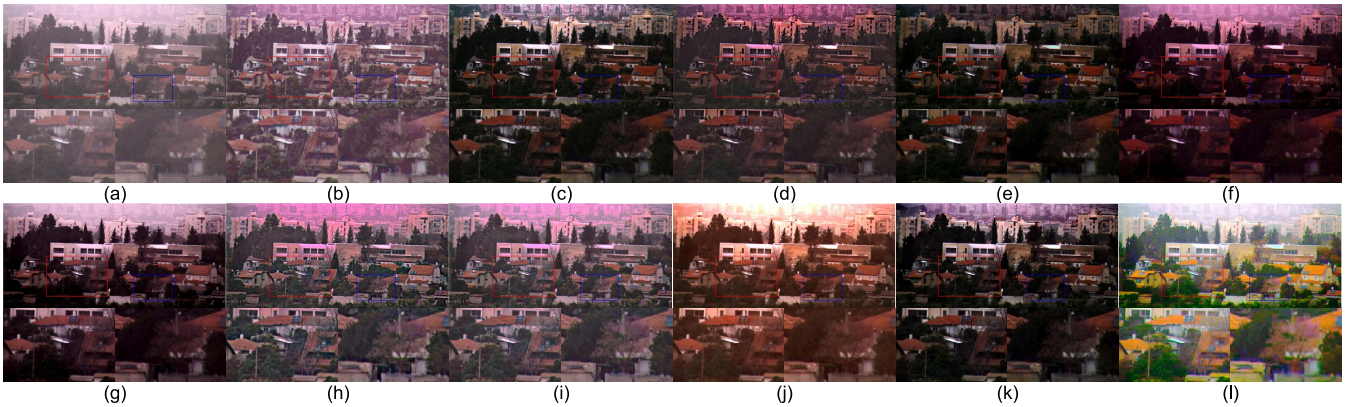

FIGURE 8. Subjective comparisons of different methods on images: (a) Input hazy image, (b) FVR, (c) DCP, (d) BCCR, (e) ATM, (f) CAP, (g) DehazeNet, (h) PADMEF, (i) Zhu *et al.*, (j) Zhao *et al.*, (k) Li *et al.*, and (l) Our MCPA.

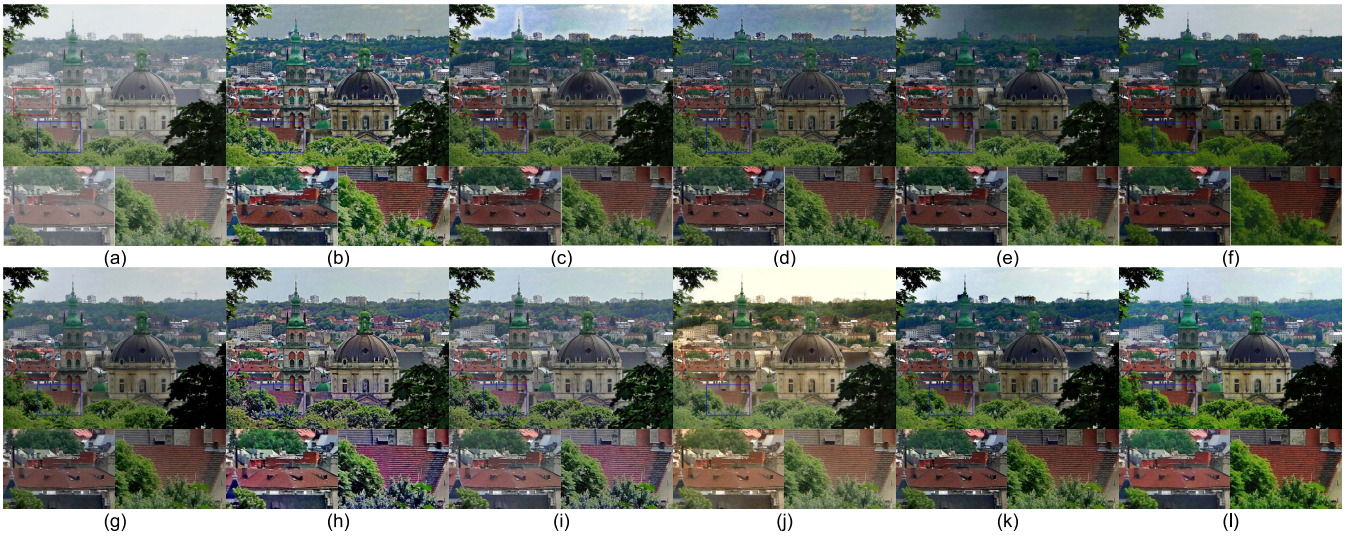

FIGURE 9. Subjective comparisons of different methods on images: (a) Input hazy image, (b) FVR, (c) DCP, (d) BCCR, (e) ATM, (f) CAP, (g) DehazeNet, (h) PADMEF, (i) Zhu *et al.*, (j) Zhao *et al.*, (k) Li *et al.*, and (l) Our MCPA.

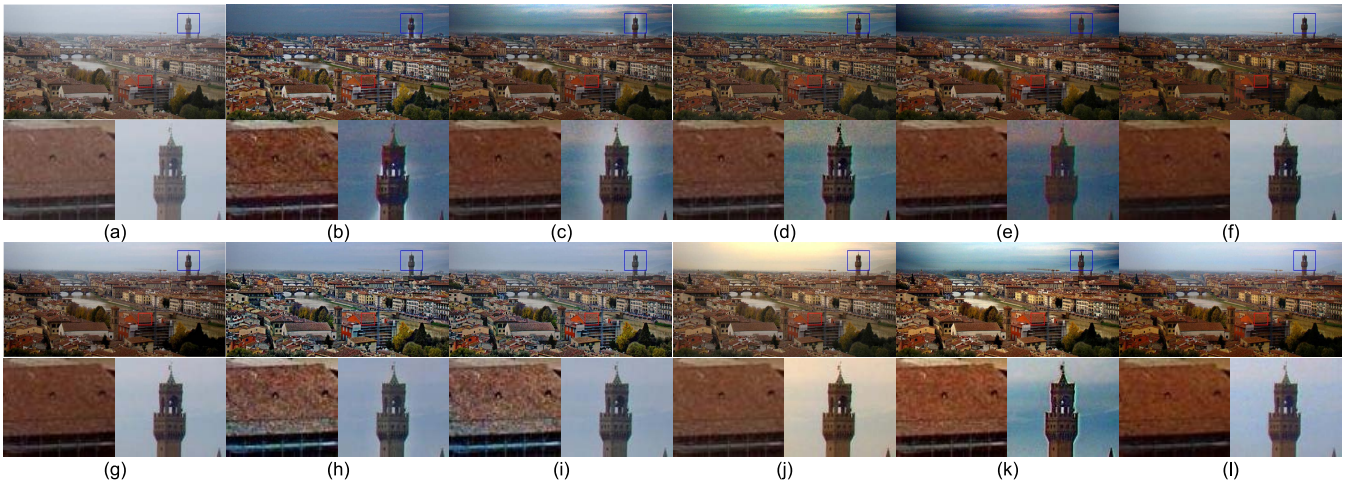

FIGURE 10. Subjective comparisons of different methods on images: (a) Input hazy image, (b) FVR, (c) DCP, (d) BCCR, (e) ATM, (f) CAP, (g) DehazeNet, (h) PADMEF, (i) Zhu *et al.*, (j) Zhao *et al.*, (k) Li *et al.*, and (l) Our MCPA.

in the darkening of some areas, where the train of Fig. 5(e) and the rails of Fig. 5(f) even become inconspicuous. The method of Figs. 5(h) and 5(i) can successfully remove haze. Fig. 5(l) shows that our proposed method (MCPA) successfully removes haze. Also, our proposed method can restore the color of the green trees, as shown in the enlarged image, better than other advanced state-of-the-art haze removal methods.

Fig. 6(a) has rich color information, so the degree of color recovery can be seen from different dehazing methods. It can be seen from the methods shown in Figs. 6(b), 6(g), and 6(i) that the haze has not been effectively processed, and the image still remains in the area of white haze. Figs. 6(c) and 6(h) show that both DCP and PADMEF can effectively remove haze, and the color recovery is as good as our proposed method. Figs. 6(e), 6(f), and 6(k) show the results that some areas become darkened, such as the area in the lower-left corner of the image. In Figs. 6(d) and 6(j), the color is distorted, although the dehazing effect is good. As shown in Fig. 6(l), our proposed method (MCPA) can restore the image with high color saturation and recover the image's color successfully, as shown in the enlarged image.

As shown in Figs. 7(b)-7(d), halo artifacts appear in the middle branch. Figs. 7(e) and 7(j) produce unreal tones. Although Fig. 7(f) has a good dehazing effect, it produces dark areas in the image, and the loss of details can be seen from the enlarged image. In Figs. 7(g) and 7(k) the degree of color restoration is significantly lower than our method. Figs. 7(h) and 7(i) produce good sharpened edges. Fig. 7(l) shows that our method does not cause halo artifacts and is much better than most state-of-the-art methods, as shown in the enlarged image.

The hazy area in Fig. 8(a) is reddish, which may be caused by the high color temperature of the scene at that time or the problem of the color balance setting of the camera when capturing. Most state-of-the-art dehazing algorithms cannot restore the image's color, instead causing the image's color balance to be out of balance. As shown in Figs. 8(b)-8(d) and 8(f)-8(i), the hazy areas in the upper part of the images become redder than that in Fig. 8(a). The overall color of the scene in Fig. 8(j) varies too much, resulting in incongruent colors. Fig. 8(k) shows that the buildings in the fog can be restored, but the trees below buildings are too dark. Although the recovered colors in Fig. 8(e) are not distorted, the image is too dark, and details are lost. As shown in Fig. 8(l), our proposed method (MCPA) not only does not over-enhance the reddish color of the foggy area of the original image in Fig. 8(a), but also enhances the darker areas of the original image to become brighter and more detailed as shown in the enlarged image.

Hazy natural images or objects of white scenes have always been a major obstacle to removing haze. Fig. 9(a) has a sky region with dense trees and buildings. Many dehazing algorithms cannot effectively deal with sky areas, causing sky color distortion or artifacts, as shown in Figs. 9(b)-(e), and 9(j). Although Figs. 9(f) and 9(k) can effectively remove the fog, but they still cause the image to be partially dark. The defogging effect of Fig. 9(g) is relatively weak, so the trees' color is not bright enough. Fig. 9(h) produces good sharpened edges. The color restoration of Fig. 9(i) is not as vivid as our method. Fig. 9(l) shows that our method removes haze well and recovers the most vividness of colors better than most advanced state-of-the-art haze removal methods, such as the red roof shown in the enlarged image.

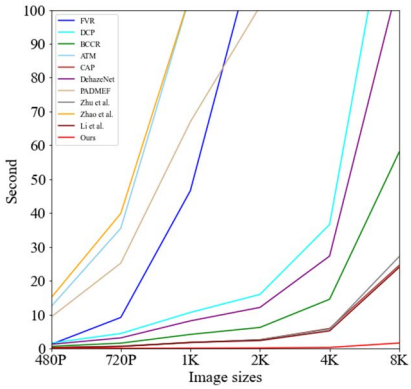

FIGURE 11. Comparisons of different methods on computational processing speed.

Fig. 10(a) is a sky image with many white clouds. Many dehazing algorithms cannot effectively deal with sky areas, causing sky color distortion or artifacts, as shown in Figs. 10(b)-(e), and 10(j). Although Fig. 10(f) can effectively remove the fog, they still cause the image to be partially dark. The color restoration of Fig. 10(g) is not as vivid as our method. The enlarged image shows that Figs. 10(h)-10(i) show that both PADME and Zhu can successfully remove haze and restore color. Figs. 10(b)-(e), and 10(k) show that the tower of the enlarged image produces halo artifacts. Fig. 10(l) shows that our method not only does not produce halo artifacts in the sky, but also no noise in the details.

B. OBJECTIVE QUALITY ASSESSMENTS

Table 1 shows that 100 hazy images are collected and evaluated the state-of-the-art methods and our method on the average score of the 100 hazy images for eight image quality metrics. The eight image quality metrics include the Peak Signal to Noise Ratio (PSNR), Mean Squared Error (MSE), the Structural Similarity (SSIM) [62], the Feature SIMilarity (FSIM) [63], the Information Entropy (IE), the rate of visible edges numbers e, the ratio of the gradients at visible edges $\bar{r}$, and the percentage Σ of completely black or completely white pixels after restoration.

The PSNR indicates that the peak signal-to-noise ratio reflects the distortion of the image. The larger the peak signal-to-noise ratio, the smaller the image distortion. The MSE represents the sum of the differences between the pixels in the two images. The smaller the value of MSE, the closer the two images are. The SSIM index and FSIM are used to measure the similarity of two images. The larger the index value, the more similar the images are and the less distortion. The quality of the dehazing results is also judged through the IE, which is the average condition of the information in the image. The larger the information entropy is, the more detailed information the image contains. In addition to this, the method proposed in [64] dedicated to evaluating visibility recovery is used. The method calculates three indicators respectively, including the rate of visible edges numbers e, the ratio of

TABLE 1. Average objective quality results based on different methods. ↑ the higher the better; ↓ the lower the better; Bold: the best.

	FVR	DCP	BCCR	ATM	CAP	DehazeNet	PADMEF	Zhu et al.	Zhao et al.	Li et al.	Ours
PSNR ↑	13.528	14.770	14.214	11.536	14.361	17.030	15.752	17.749	18.976	12.306	**19.209**
MSE ↓	2698.714	2182.785	2276.479	5867.486	2583.393	1256.718	1875.504	1186.235	1316.783	4049.331	**976.384**
SSIM ↑	0.734	0.727	0.737	0.637	0.662	0.729	0.677	0.724	0.625	0.645	**0.770**
FSIM ↑	0.853	0.925	0.910	0.842	0.910	**0.972**	0.830	0.890	0.851	0.850	0.957
Entropy ↑	7.296	7.359	7.215	6.711	7.121	7.217	7.514	7.479	7.316	7.466	**7.877**
e ↑	1.059	**1.153**	0.966	1.083	0.462	0.459	0.840	0.748	0.281	0.871	0.873
$\bar{r}$ ↑	**2.303**	1.788	1.853	1.7	1.074	1.214	2.198	1.995	1.361	1.933	1.709
Σ ↓	0.022	0.010	0.014	0.012	0.035	0.107	0.013	0.007	**0.000**	0.024	0.030

TABLE 2. Time consumption ↓ (second) comparison with state-of-the-art methods.

	FVR	DCP	BCCR	ATM	CAP	DehazeNet	PADMEF	Zhu et al.	Zhao et al.	Li et al.	Ours
8K	7246.995	150.166	58.022	-	24.551	109.015	1039.030	27.140	1410.077	23.938	**1.593**
4K	583.880	36.594	14.522	440.912	5.894	27.274	230.961	5.697	355.800	5.180	**0.294**
2K	124.222	15.951	6.194	161.393	2.563	12.115	101.044	2.579	157.352	2.312	**0.138**
1K	46.601	10.627	4.139	104.377	1.707	8.138	66.952	1.765	104.623	1.786	**0.091**
720P	9.145	4.396	1.555	35.478	0.601	3.109	25.182	0.679	39.865	0.564	**0.044**
480P	1.210	1.569	0.617	12.370	0.245	1.219	9.287	0.250	14.982	0.205	**0.025**
AVG.	1335.342	36.551	14.175	-	5.927	26.812	245.409	6.352	347.117	5.664	**0.366**

the gradients at visible edges $\bar{r}$, and the percentage Σ of completely black or completely white pixels after restoration.

From the results, the PSNR, MSE, and IE of our method are the best, which verifies that our results have the least noise, and the closer the image is to the ground truth. On the contrary, the performance of ATM in PSNR, MSE, and IE is the worst due to the excessive enhancement, noise, and image distortion. A higher value of SSIM indicates high similarity between the dehazed image and the ground truth image, while a lower value of SSIM indicates the opposite. The SSIM values for ATM, CAP, PADMEF, Zhao *et al*., and Li *et al*. were all below 0.7, indicating that much structural information had been lost in the enhanced images. Among the performance of FSIM, DehazeNet achieves the highest score, which indicates the closest structural and feature similarity to the original image. However, our method is very close to the FSIM value of DehazeNet, indicating that our method can also effectively extract features. The larger the value e, the greater the enhancement of the number of visible edges in the image. The values e of FVR, DCP, BCCR, and ATM are the closest and significantly higher than our method. However, from Figs. 7(b)-(e), it can be seen that there are apparent halo artifacts in the edges and corners, and there are spurious edges and much noise in the sky area, which is the reason for their large visible edge detection e. The value of e in our method is ranked around the middle, which indicates that our method does not produce over-sharpened edges. The $\bar{r}$ indicates that the degree of image gradient enhancement represents the degree of restoration of image edge and texture information. Although the $\bar{r}$ value of FVR is the largest, and it can be seen from Fig. 4(b) that over-enhancing the edges makes the girl's face appear strong local contrast. Although CAP does not produce too much image sharpening because the value of $\bar{r}$ is minimal. However, the image details are lost. For example, the rails at the bottom of Fig. 5(f) are not obvious. From a subjective perspective, our method does not cause excessive image sharpening or loss of image details. A lower Σ value maintains a lower percentage of all black or all white pixels, which results in more natural, sharp edges and richer colors. Objective visual shows that Zhao *et al*. performed the best at Σ values. But from the subjective vision, Figs. 4(j), 5(j), 6(j), 7(j), and 8(j) not only have a poor defogging effect but also enhance the color of the fog, causing the image color to be incongruous. Although our method does not get the best score in FSIM, e, $\bar{r}$, and Σ, compared with other image evaluation quality, such as PSNR, MSE, and SSIM, our method is significantly better. The results of our method show that dehazed images reproduce more natural colors (with little color distortion) and show sharper details. At the same time, our method minimizes artifacts and makes the image subjectively visually similar to the ground truth due to a patchless approach.

C. TIME ASSESSMENTS

In Table 2 and Fig. 11, the average running time of FVR [59], DCP [6] (accelerated by the guided image filtering [57]), BCCR [12], ATM [13], CAP [24], DehazeNet [39], PADMEF [19], Zhu *et al*. [20], Li *et al*. [21], and Zhao *et al*. [22] are evaluated. The state-of-the-art methods in the experiment use the official open-source codes of the Matlab version and use the default parameters to compare estimated time consumption. Different image sizes, including 8K (7,680 × 4.320 pixels), 4K (3,840 × 2.160 pixels), 2K (2,560 × 1.440 pixels), 1K (1,920 × 1.080 pixels), 720P (1,280 × 720 pixels), 480P (720 × 480 pixels) are used, and 100 hazy images are collected and resized to calculate the average running time. From the results, the operation time of ATM is the longest because the use of local patches and the calculation

of the atmospheric light color vector are too complicated, resulting in an excessive computational burden on the image. In addition, the operation time of ATM in 8K images is too long, which causes memory overflow and cannot run 8K images because of the computer specifications in this experiment. Our proposed method is the fastest among all methods and all image sizes and can be implemented in real-time applications. Even on 8K images, it only takes 1.5 seconds on average, about 15 times faster than the second-fastest Li *et al*. [21]. It is noted that the fast image dehazing method proposed by Wang *et al*. [14] can also achieve very high computational processing speed as fast as the proposed method. Due to the fact that filtering algorithms in patch-based image haze removal methods take too much computation time. The proposed method can significantly reduce computation time because it uses a patchless approach that does not need any filter or complicated algorithms.

V. CONCLUSION

This paper proposes a fast single image haze removal method based on a minimum channel and patchless approach. A new simple approach to estimate the atmospheric light and the scene transmission is proposed based on the minimum channel of images. The histogram of the minimum channel of the image is used to extract the atmospheric light pixels and exclude the non-hazy bright pixels in the image. The histogram equalization and image multiplication are applied to achieve better visual quality. Experimental results show that our proposed method outperforms most current state-of-the-art haze removal algorithms using qualitative and quantitative evaluations and can achieve better visual quality. Also, our proposed method is the fastest among the up-to-date state-of-the-art haze removal methods and is about 15 times faster than the second-fastest method. Our proposed method has a significant advantage in computation time because it uses a patchless approach that does not need any filter and complicated computations. Due to estimating the atmospheric light accurately, most colors of images can be restored. From subjective vision, the proposed method can restore more rich colors and make the image look natural. Also, our proposed method can automatically perform haze removal for all types of hazy mages without presetting its processing parameter values. According to the analysis of time assessment, our proposed method can be implemented in a mobile device with limited resources. Although the proposed dehazing method can restore the vividness of the image's colors, it may over-enhance the image in some cases. This limitation might be solved in future studies by considering the type of haze.

REFERENCES

[1] T. K. Kim, J. K. Paik, and B. S. Kang, "Contrast enhancement system using spatially adaptive histogram equalization with temporal filtering," *IEEE Trans. Consum. Electron.*, vol. 44, no. 1, pp. 82–87, Feb. 1998.
[2] J. A. Stark, "Adaptive image contrast enhancement using generalizations of histogram equalization," *IEEE Trans. Image Process.*, vol. 9, no. 5, pp. 889–896, May 2000.
[3] J.-Y. Kim, L.-S. Kim, and S.-H. Hwang, "An advanced contrast enhancement using partially overlapped sub-block histogram equalization," *IEEE Trans. Circuits Syst. Video Technol.*, vol. 11, no. 4, pp. 475–484, Apr. 2001.
[4] R. T. Tan, "Visibility in bad weather from a single image," in *Proc. IEEE Conf. Comput. Vis. Pattern Recognit.*, Anchorage, AK, USA, Jun. 2008, pp. 1–8.
[5] R. Fattal, "Single image dehazing," *ACM Trans. Graph.*, vol. 27, no. 3, pp. 1–9, 2008.
[6] K. He, J. Sun, and X. Tang, "Single image haze removal using dark channel prior," *IEEE Trans. Pattern Anal. Mach. Intell.*, vol. 33, no. 12, pp. 2341–2353, Dec. 2011.
[7] Y. Iwamoto, N. Hashimoto, and Y.-W. Chen, "Real-time haze removal using normalised pixel-wise dark-channel prior and robust atmospheric-light estimation," *Appl. Sci.*, vol. 10, no. 3, p. 1165, Feb. 2020.
[8] Y. R. Musunuri and O.-S. Kwon, "Haze removal based on refined transmission map for aerial image matching," *Appl. Sci.*, vol. 11, no. 15, p. 6917, Jul. 2021.
[9] Y.-T. Peng, Z. Lu, F.-C. Cheng, Y. Zheng, and S.-C. Huang, "Image haze removal using airlight white correction, local light filter, and aerial perspective prior," *IEEE Trans. Circuits Syst. Video Technol.*, vol. 30, no. 5, pp. 1385–1395, May 2020.
[10] Z. G. Li and J. H. Zheng, "Single image de-hazing using globally guided image filtering," *IEEE Trans. Image Process.*, vol. 27, no. 1, pp. 442–450, Jan. 2018.
[11] J. Yu, C. Xiao, and D. Li, "Physics-based fast single image fog removal," in *Proc. IEEE 10th Int. Conf. Signal Process.*, Beijing, China, Oct. 2010, pp. 1048–1052.
[12] G. Meng, Y. Wang, J. Duan, S. Xiang, and C. Pan, "Efficient image dehazing with boundary constraint and contextual regularization," in *Proc. IEEE Int. Conf. Comput. Vis.*, Sydney, NSW, Australia, Dec. 2013, pp. 617–624.
[13] M. Sulami, I. Glatzer, R. Fattal, and M. Werman, "Automatic recovery of the atmospheric light in hazy images," in *Proc. IEEE Int. Conf. Comput. Photography (ICCP)*, Santa Clara, CA, USA, May 2014, pp. 1–11.
[14] W. Wang, X. Yuan, X. Wu, and Y. Liu, "Fast image dehazing method based on linear transformation," *IEEE Trans. Multimedia*, vol. 19, no. 6, pp. 1142–1155, 2017.
[15] T. Zhang, H. Hu, and B. Li, "A naturalness preserved fast dehazing algorithm using HSV color space," *IEEE Access*, vol. 6, pp. 10644–10649, 2018.
[16] A. Khmag, S. A. R. Al-Haddad, A. R. Ramli, and B. Kalantar, "Single image dehazing using second-generation wavelet transforms and the mean vector L2-norm," *Vis. Comput.*, vol. 34, no. 5, pp. 675–688, May 2018.
[17] J. Shin, M. Kim, J. Paik, and S. Lee, "Radiance-reflectance combined optimization and structure-guided ℓ_0-norm for single image dehazing," *IEEE Trans. Multimedia*, vol. 22, no. 1, pp. 30–44, Jan. 2020.
[18] H.-M. Hu, H. Zhang, Z. Zhao, B. Li, and J. Zheng, "Adaptive single image dehazing using joint local-global illumination adjustment," *IEEE Trans. Multimedia*, vol. 22, no. 6, pp. 1485–1495, Jun. 2020.
[19] M. Zheng, G. Qi, Z. Zhu, Y. Li, H. Wei, and Y. Liu, "Image dehazing by an artificial image fusion method based on adaptive structure decomposition," *IEEE Sensors J.*, vol. 20, no. 14, pp. 8062–8072, Jul. 2020.
[20] Z. Zhu, H. Wei, G. Hu, Y. Li, G. Qi, and N. Mazur, "A novel fast single image dehazing algorithm based on artificial multiexposure image fusion," *IEEE Trans. Instrum. Meas.*, vol. 70, pp. 1–23, 2021.
[21] Z. Li, H. Shu, and C. Zheng, "Multi-scale single image dehazing using Laplacian and Gaussian pyramids," *IEEE Trans. Image Process.*, vol. 30, pp. 9270–9279, 2021.
[22] X. Zhao, "Single image dehazing using bounded channel difference prior," in *Proc. IEEE/CVF Conf. Comput. Vis. Pattern Recognit. Workshops (CVPRW)*, Jun. 2021, pp. 727–735.
[23] K. Tang, J. Yang, and J. Wang, "Investigating haze-relevant features in a learning framework for image dehazing," in *Proc. IEEE Conf. Comput. Vis. Pattern Recognit.*, Columbus, OH, USA, Jun. 2014, pp. 2995–3002.
[24] Q. Zhu, J. Mai, and L. Shao, "A fast single image haze removal algorithm using color attenuation prior," *IEEE Trans. Image Process.*, vol. 24, no. 11, pp. 3522–3533, Nov. 2015.
[25] D. Ngo, G.-D. Lee, and B. Kang, "Improved color attenuation prior for single-image haze removal," *Appl. Sci.*, vol. 9, no. 19, p. 4011, Sep. 2019.
[26] D. H. Kim, W. J. Ahn, M. T. Lim, T. K. Kang, and D. W. Kim, "Frequency-based haze and rain removal network (FHRR-Net) with deep convolutional encoder–decoder," *Appl. Sci.*, vol. 11, no. 6, p. 2873, Mar. 2021.
[27] Q. Bu, J. Luo, K. Ma, H. Feng, and J. Feng, "An enhanced pix2pix dehazing network with guided filter layer," *Appl. Sci.*, vol. 10, no. 17, p. 5898, Aug. 2020.
[28] H. Dong, J. Pan, L. Xiang, Z. Hu, X. Zhang, F. Wang, and M.-H. Yang, "Multi-scale boosted dehazing network with dense feature fusion," 2020, *arXiv:2004.13388*.

[29] L. He, J. Bai, and L. Ru, "Haze removal using aggregated resolution convolution network," *IEEE Access*, vol. 7, pp. 123698–123709, 2019.
[30] S. Tangsakul and S. Wongthanavasu, "Single image haze removal using deep cellular automata learning," *IEEE Access*, vol. 8, pp. 103181–103199, 2020.
[31] Y. Li, J. Ren, and Y. Huang, "An end-to-end system for unmanned aerial vehicle high-resolution remote sensing image haze removal algorithm using convolution neural network," *IEEE Access*, vol. 8, pp. 158787–158797, 2020.
[32] J. Yan, C. Li, Y. Zheng, S. Xu, and X. Yan, "MMP-Net: A multi-scale feature multiple parallel fusion network for single image haze removal," *IEEE Access*, vol. 8, pp. 25431–25441, 2020.
[33] S. A. Hovhannisyan, H. A. Gasparyan, S. S. Agaian, and A. Ghazaryan, "AED-Net: A single image dehazing," *IEEE Access*, vol. 10, pp. 12465–12474, 2022.
[34] D. Yang and J. Sun, "A model-driven deep dehazing approach by learning deep priors," *IEEE Access*, vol. 9, pp. 108542–108556, 2021.
[35] Y. Pang, J. Nie, J. Xie, J. Han, and X. Li, "BidNet: Binocular image dehazing without explicit disparity estimation," in *Proc. IEEE/CVF Conf. Comput. Vis. Pattern Recognit. (CVPR)*, Jun. 2020, pp. 5931–5940.
[36] Z. Zhou, Z. Shi, M. Guo, Y. Feng, and M. Zhao, "CGGAN: A context guided generative adversarial network for single image dehazing," 2020, *arXiv:2005.13884*.
[37] X. Qin, Z. Wang, Y. Bai, X. Xie, and H. Jia, "FFA-Net: Feature fusion attention network for single image dehazing," in *Proc. AAAI Conf. Artif. Intell.*, 2020, pp. 11908–11915.
[38] C. Wang, Z. Li, J. Wu, H. Fan, G. Xiao, and H. Zhang, "Deep residual haze network for image dehazing and deraining," *IEEE Access*, vol. 8, pp. 9488–9500, 2020.
[39] B. L. Cai, X. M. Xu, K. Jia, C. M. Qing, and D. C. Tao, "Dehazenet: An end-to-end system for single image haze removal," *IEEE Trans. Image Process*, vol. 25, no. 11, pp. 5187–5198, Aug. 2016.
[40] W. Ren, S. Liu, H. Zhang, J. Pan, X. Cao, and M. H. Yang, "Single image dehazing via multi-scale convolutional neural networks," in *Proc. 14th Eur. Conf. Comput. Vis.*, Amsterdam, The Netherlands, 2016, pp. 154–169.
[41] S. Lee, S. Yun, J.-H. Nam, C. S. Won, and S.-W. Jung, "A review on dark channel prior based image dehazing algorithms," *EURASIP J. Image Video Process.*, vol. 2016, no. 1, pp. 1–23, Dec. 2016.
[42] H. Yang and J. Wang, "Color image contrast enhancement by co-occurrence histogram equalization and dark channel prior," in *Proc. 3rd Int. Cong. Image Signal Process.*, Yantai, China, 2010, pp. 659–663.
[43] M. Sandeep, "Remote sensing image dehazing using guided filter," *Int. J. Res. Stud. Comput. Sci. Eng.*, vol. 1, no. 3, pp. 44–49, 2014.
[44] J. Long, Z. Shi, and W. Tang, "Fast haze removal for a single remote sensing image using dark channel prior," in *Proc. Int. Conf. Comput. Vis. Remote Sens.*, Xiamen, China, Dec. 2012.
[45] H. Xu, J. Guo, Q. Liu, and L. Ye, "Fast image dehazing using improved dark channel prior," in *Proc. IEEE Int. Conf. Inf. Sci. Technol.*, Wuhan, China, Mar. 2012, pp. 663–667.
[46] X. Lv, W. Chen, and I.-F. Shen, "Real-time dehazing for image and video," in *Proc. 18th Pacific Conf. Comput. Graph. Appl.*, Hangzhou, China, Sep. 2010, pp. 62–69.
[47] C. Xiao and J. Gan, "Fast image dehazing using guided joint bilateral filter," *Vis. Comput.*, vol. 28, nos. 6–8, pp. 713–721, Jun. 2012.
[48] B. Zhang and J. Wei, "Hardware implementation for haze removal with adaptive filtering," *IEEE Access*, vol. 7, pp. 142498–142506, 2019.
[49] Y. Linan, P. Yan, and Y. Xiaoyuan, "Video defogging based on adaptive tolerance," *TELKOMNIKA Indonesian J. Electr. Eng.*, vol. 10, no. 7, pp. 1644–1654, Nov. 2012.
[50] Z. Lin, "Dehazing for image and video using guided filter," *Open J. Appl. Sci.*, vol. 2, no. 4, pp. 123–127, 2012.
[51] Y. Zou, Y. Ma, L. Zhuang, and G. Wang, "Image haze removal algorithm using a logarithmic guide filtering and multi-channel prior," *IEEE Access*, vol. 9, pp. 11416–11426, 2021.
[52] N. Hautière, J.-P. Tarel, J. Lavenant, and D. Aubert, "Automatic fog detection and estimation of visibility distance through use of an onboard camera," *Mach. Vis. Appl.*, vol. 17, no. 1, pp. 8–20, Apr. 2006.
[53] A. Levin, D. Lischinski, and Y. Weiss, "A closed-form solution to natural image matting," *IEEE Trans. Pattern Anal. Mach. Intell.*, vol. 30, no. 2, pp. 228–242, Feb. 2008.
[54] K. B. Gibson, D. T. Vo, and T. Q. Nguyen, "An investigation of dehazing effects on image and video coding," *IEEE Trans. Image Process.*, vol. 21, no. 2, pp. 662–673, Feb. 2012.
[55] F. C. Cheng, C. H. Lin, and J. L. Lin, "Constant time O(1) image fog removal using lowest level channel," *Electron. Lett.*, vol. 48, no. 22, pp. 1404–1405, 2012.
[56] B.-H. Chen, S.-C. Huang, and F.-C. Cheng, "A high-efficiency and high-speed gain intervention refinement filter for haze removal," *J. Display Technol.*, vol. 12, no. 7, pp. 753–759, Jul. 2016.
[57] K. He, J. Sun, and X. Tang, "Guided image filtering," *IEEE Trans. Pattern Anal. Mach. Intell.*, vol. 35, no. 6, pp. 1397–1409, Jun. 2013.
[58] R. C. Gonzalez and R. E. Woods, *Digital Image Processing*. Upper Saddle River, NJ, USA: Prentice-Hall, 2008.
[59] J.-P. Tarel and N. Hautiere, "Fast visibility restoration from a single color or gray level image," in *Proc. IEEE 12th Int. Conf. Comput. Vis.*, Kyoto, Japan, Sep. 2009, pp. 2201–2208.
[60] C. Ancuti, C. O. Ancuti, R. Timofte, and C. D. Vleeschouwer, "I-HAZE: A dehazing benchmark with real hazy and haze-free indoor images," in *Proc. Int. Conf. Adv. Concepts Intell. Vis. Syst.*, 2018, pp. 620–631.
[61] C. O. Ancuti, C. Ancuti, R. Timofte, and C. De Vleeschouwer, "O-HAZE: A dehazing benchmark with real hazy and haze-free outdoor images," in *Proc. IEEE/CVF Conf. Comput. Vis. Pattern Recognit. Workshops (CVPRW)*, Jun. 2018, pp. 754–762.
[62] Z. Wang, A. C. Bovik, H. R. Sheikh, and E. P. Simoncelli, "Image quality assessment: From error visibility to structural similarity," *IEEE Trans. Image Process.*, vol. 13, no. 4, pp. 600–612, Apr. 2004.
[63] L. Zhang, L. Zhang, X. Mou, and D. Zhang, "FSIM: A feature similarity index for image quality assessment," *IEEE Trans. Image Process.*, vol. 20, no. 8, pp. 2378–2386, Aug. 2011.
[64] N. Hautière, J.-P. Tarel, D. Aubert, and É. Dumont, "Blind contrast enhancement assessment by gradient ratioing at visible edges," *Image Anal. Stereol.*, vol. 27, no. 2, p. 87, May 2011.

CHIOU-SHANN FUH (Member, IEEE) received the B.S. degree in computer science and information engineering from National Taiwan University, Taipei, in 1983, the M.S. degree in computer science from Pennsylvania State University, University Park, in 1987, and the Ph.D. degree in computer science from Harvard University, Cambridge, MA, USA, in 1992. He was at AT&T Bell Laboratories, where he was engaged in performance monitoring of switching networks, from 1992 to 1993. He was an Associate Professor at the Department of Computer Science and Information Engineering, National Taiwan University, Taipei, from 1993 to 2000, and was then promoted to a Full Professor. His current research interests include digital image processing, computer vision, pattern recognition, mathematical morphology, and their applications to defect inspection, industrial automation, digital still camera, digital video camcorder, and camera module, such as artificial intelligence, machine learning, deep learning, color interpolation, auto exposure, auto focus, auto white balance, color calibration, and color management.

TZU-CHIA TUNG received the B.S. degree in computer science and information engineering from Chung Hua University, in 2012, and the M.S. degree in computer science and information engineering from National Dong Hwa University, in 2016. He is currently pursuing the Ph.D. degree with Graduate Institute of Networking and Multimedia, National Taiwan University. His research interests include computer vision, image processing, pattern recognition, and machine learning.